



Original Article

Conceptual design of a 3D-Printable DC electromagnetic pump for additive manufacturing

Geunhyeong Lee¹

Korea Atomic Energy Research Institute, Applied Artificial Intelligence Lab, Daejeon, 34057, Republic of Korea

ARTICLE INFO

Keywords:
 Metal 3D printing
 Electromagnetic pump
 Direct current
 Multiple lorentz forces
 Design for additive manufacturing (DfAM)

ABSTRACT

Electromagnetic pumps offer advantages in handling high-temperature or corrosive fluids by generating flow through Lorentz forces rather than mechanical impellers. However, direct current electromagnetic pumps typically require large currents, resulting in increased manufacturing costs due to thicker copper wires. This study proposes a novel direct current electromagnetic pump for metal additive manufacturing, potentially suitable for advanced Small Modular Reactors cooled by liquid sodium and liquid-metal charge stripper systems used in accelerators. Permanent magnets arranged in opposing directions generate concentrated magnetic flux around constrained flow paths, thereby producing multiple Lorentz forces and reducing the required input current. Numerical simulations demonstrate that the proposed design achieves a developed pressure of 10.5 bar at a significantly reduced current of 330 A, corresponding to a 52 % reduction in current compared to conventional helical-type pumps operating under similar conditions. Additionally, the new pump geometry simplifies fabrication by eliminating brazed joints and enabling a more compact design. These results indicate that 3D-printable electromagnetic pumps provide improvements in performance and ease of fabrication for high-pressure applications.

1. Introduction

Small Modular Reactors (SMRs) and Generation IV nuclear reactors utilizing liquid-metal coolants, such as sodium or lead–bismuth eutectic (LBE), have renewed interest in the development and application of electromagnetic (EM) pumps for coolant circulation [1–3]. EM pumps drive electrically conductive fluids using Lorentz forces, eliminating mechanical impellers and seals. This provides significant advantages, including reliable high-temperature operation, reduced maintenance, and minimal leak risks, making them especially beneficial for nuclear systems handling reactive or corrosive fluids [4,5]. Consequently, EM pumps have been successfully deployed in primary and secondary coolant loops in sodium-cooled fast reactors, LBE-cooled reactors, and liquid-metal charge stripper systems for heavy-ion accelerators [4–6].

Beyond nuclear applications, EM pumps are also employed in metallurgical processes, such as continuous steel casting and aluminum refining, where electromagnetic forces effectively control molten metal flow and enhance product quality [7,8]. Recently, EM pump technology has expanded into advanced thermal management systems for high heat-flux electronics and energy devices, highlighting their capability to

effectively manage challenging thermal conditions [9]. This expansion is largely driven by the significant potential of liquid metals as superior coolants, a topic covered extensively in recent experimental and analytical studies [10,11].

Among the various types of EM pumps, direct-current (DC) pumps are a significant category, operating on the conduction principle where an electric current is directly supplied to the fluid perpendicular to a magnetic field. Compared to their alternating-current (AC) induction counterparts, which require complex windings, DC pumps feature a simpler construction that enhances reliability and allows for more precise flow control. However, the primary challenge of traditional DC pumps is their reliance on high electric currents to generate substantial Lorentz forces, leading to high power consumption and complex cooling requirements. To address this limitation, research has focused on innovative pump geometries. For instance, Yao et al. introduced a design with a Halbach magnet array to improve magnetic flux concentration [12], while Sun et al. developed a compact double-spiral pump for high-pressure generation [13]. Among the more fundamental geometries, such as rectangular, cylindrical, and helical types, a systematic comparison by Lee demonstrated that the helical-type pump was

E-mail address: leeg@rib.msu.edu.¹ (Present affiliation: Facility for Rare Isotope Beams, High Power Targetry Team, East Lansing, MI, 48824, USA).

particularly effective. It required only 9 % of the current needed by the other types to achieve identical performance, establishing it as an efficient benchmark for DC EM pumps [14].

Despite their advantages, conventional helical-type electromagnetic pumps face practical implementation challenges, such as complex assembly processes involving multiple brazed segments, which require precise manufacturing and specialized coatings to prevent current leakage. As illustrated in Fig. 1, brazing is essential to connect each segment of the helical flow channel, and a stop-off coating must be applied to direct the current flow appropriately. This brazing process is particularly challenging in helical channels, where inconsistent brazing can result in non-uniform current distribution and reduced operational reliability. Moreover, despite current reductions compared to other pump types, the required current levels remain relatively high.

Recent advances in additive manufacturing (AM), particularly metal 3D printing technologies such as selective laser melting, have been introduced to overcome these manufacturing hurdles by enabling monolithic fabrication of complex conductive components without joints. Studies employing stereolithography 3D printing have successfully demonstrated the fabrication of micro-scale EM pumps from magnetic nanocomposite materials, achieving complex internal geometries and significantly improved pumping performance and reliability [15,16]. Sedky and Serry further demonstrated that integrated valve mechanisms within 3D-printed EM micropumps could notably improve flow rates and power efficiency [17].

Motivated by recent advances in additive manufacturing, this study proposes a novel 3D-printable DC electromagnetic pump tailored specifically for high-performance liquid-metal coolant circulation in advanced nuclear reactor and accelerator systems. To overcome the limitations described above, this work introduces a new geometric concept. It integrates a novel magnet arrangement with a new flow channel geometry, designed specifically for metal 3D printing. This integrated design solves the key challenges of conventional helical-type pumps. The monolithic structure, made possible by 3D printing, eliminates brazed joints to simplify manufacturing. At the same time, the new configuration effectively generates multiple Lorentz forces, achieving a high-pressure output of 10.5 bar with a significantly reduced input current. The resulting design is particularly suited for next-generation nuclear and industrial applications where compactness, efficiency, and reliability are essential.

2. 3D-printable EM pump design

2.1. Working principle

Fig. 2 shows the novel conceptual design of the 3D-printable electromagnetic pump. The Lorentz force arises from the interaction between the electric current flowing through a conductive path and the magnetic flux provided by permanent magnets. A DC input enters at the top-left side of the pump and exits at the top-right side, ensuring the current follows a controlled route through the internal flow channels.

As shown in the cross-section in Fig. 3, the permanent magnets are arranged to produce opposing magnetic fields; the upper (blue) magnets generate flux in the positive y-direction, while the lower (green) magnets generate flux in the negative y-direction. The interaction of the electric current with these fields generates Lorentz forces perpendicular to the plane of the figure, directed either 'into the plane' (\otimes) or 'out of the plane' (\odot). The flow channel, detailed in Fig. 4, follows a winding path specifically designed to guide the fluid through these alternating force zones. This alignment ensures that multiple segments of Lorentz force act in series along the fluid's path, progressively building pressure from the inlet to the outlet. By effectively integrating these force segments, the total input current required to achieve high pressure is significantly reduced.

2.2. Design for additive manufacturing

The overall geometry of the pump is constrained to 180 mm \times 180 mm in width and length to reflect the build volume limitations of many commercial metal 3D printers. Fig. 3 illustrates the component intended for fabrication using metal additive manufacturing, with the build direction oriented vertically from bottom to top. To simplify fabrication and enhance surface quality, a 45° ceiling angle is applied in the upper current path section, following standard AM guidelines that recommend angles no more horizontal than 45° to avoid additional support structures.

The flow channels feature semi-cylindrical cross-sections with a diameter of 5 mm and are arranged in parallel within regions of highest magnetic flux. This design ensures sufficient cross-sectional area for fluid flow while remaining feasible for printing without excessive bridging or supports. Furthermore, each flow channel aligns closely with its corresponding current path, ensuring effective application of Lorentz forces to maximize pumping performance.

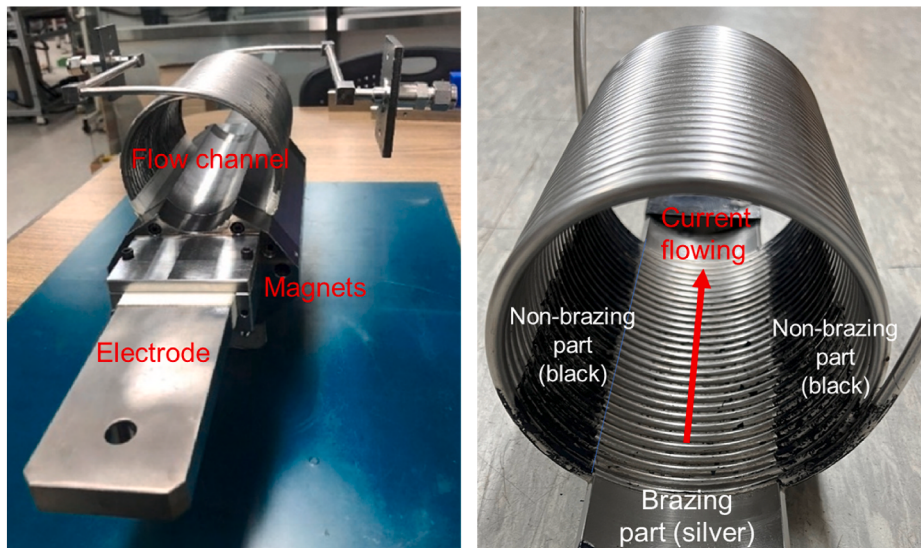


Fig. 1. Helical DC electromagnetic pump flow channel manufacturing process [6].

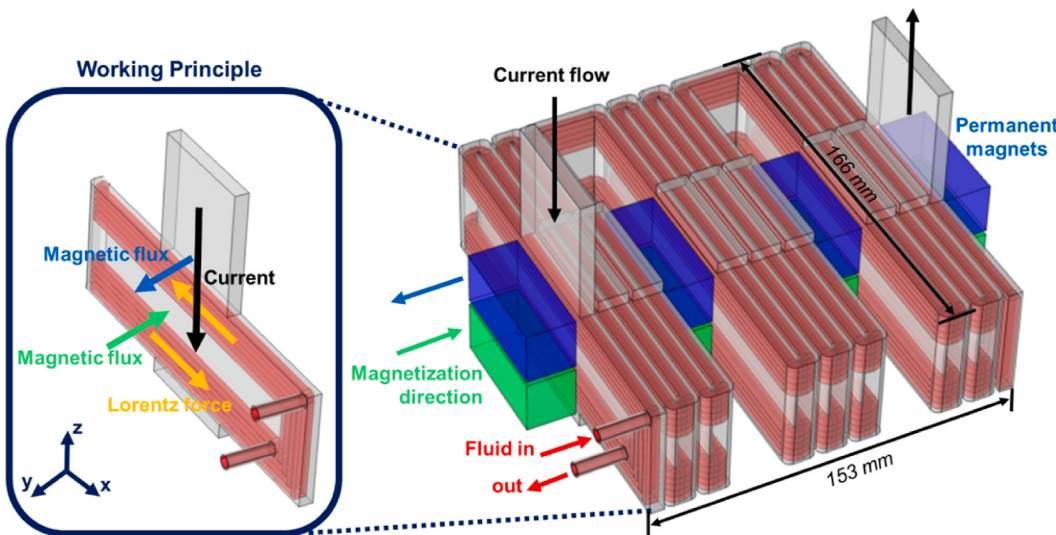


Fig. 2. 3D-printable electromagnetic pump design and working principle.

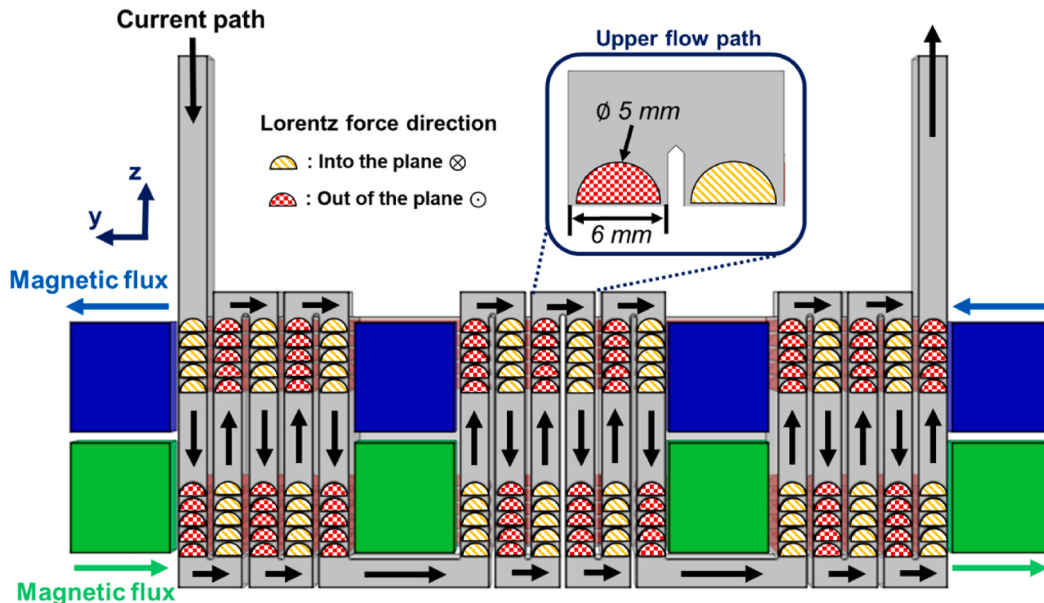


Fig. 3. Cross-sectional view (yz-plane from Fig. 2) of the pump, detailing the interaction between the current path, magnetic flux, and the resulting Lorentz force directions.

3. Methods

The 200 °C liquid lithium was selected as the working fluid, with a target pressure of 10.5 bar chosen to compare against an existing helical-type electromagnetic pump configuration for the liquid lithium charge stripper requirement. The pump's structural components, including the flow channel, were modeled using Stainless Steel 316 due to its low chemical reactivity with alkali metal. The model incorporated an electrical conductivity of 1.16×10^6 S/m [18] and a temperature-dependent thermal conductivity of 16.7 W/(m · K) at 200 °C and 18.3 W/(m · K) at 300 °C [19]. The fluid domain was specified as liquid lithium at 200 °C, featuring an electrical conductivity of 3.93×10^6 S/m, a density of 513 kg/m³, and a dynamic viscosity of 5.7×10^{-4} Pa·s [20], and thermal conductivity as 43.4 W/(m · K) [21]. Sm₂Co₁₇ (BMSG-28H) was selected for the permanent magnets owing to its high magnetic flux density and thermal stability at high temperatures.

This study employed COMSOL Multiphysics v6.2 to perform coupled

electromagnetic (EM) and fluid flow simulations under magnetohydrodynamic (MHD) conditions [22]. The overall approach integrates magnetic field calculations with fluid dynamics, reflecting the direct interaction between a flowing conductive fluid and the static magnetic field generated by permanent magnets. The resulting Lorentz force is incorporated into the Navier-Stokes equations as an additional body force.

3.1. Electromagnetic analysis

The electromagnetic analysis was conducted using COMSOL's Magnetic and Electric Fields interface under magnetostatic conditions, meaning displacement currents and time-varying fields were neglected. This interface was applied to all conductive domains, including both the solid Stainless Steel 316 pump body and the liquid lithium, to accurately model the current distribution and account for fringe currents flowing through the channel walls. Ampère's law states that the curl of the

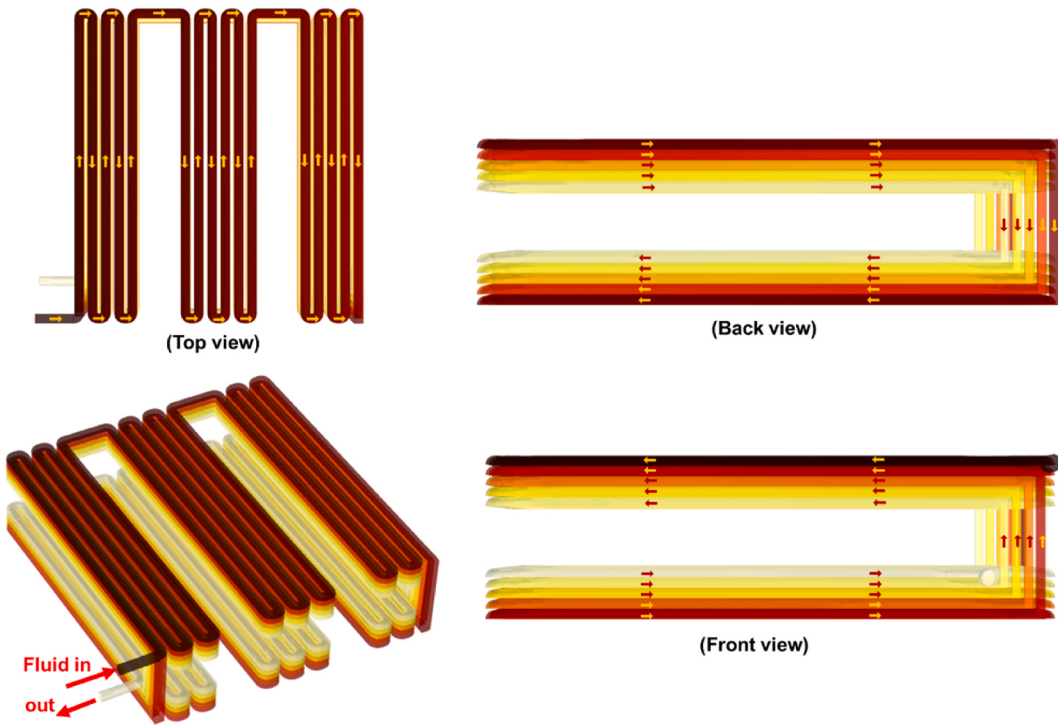


Fig. 4. Multiple views illustrating the fluid path through the flow channels.

magnetic field intensity \mathbf{H} equals the current density \mathbf{J} :

$$\nabla \times \mathbf{H} = \mathbf{J} \quad (1)$$

while current continuity ensures no net charge accumulation:

$$\nabla \cdot \mathbf{J} = 0 \quad (2)$$

The external current input boundary condition was applied as a uniform current density on the inlet cross-sectional surface of the conductive region.

3.2. Fluid flow analysis

To model the fluid domain, the flow regime was first characterized by the Reynolds number ($Re = \rho v D_h / \mu$). For the primary operating flow rate of 3 ml/s, the average velocity in the semi-circular channel is 0.3 m/s. The hydraulic diameter (D_h) for this geometry is approximately 0.003 m. Based on these parameters, the Reynolds number is calculated to be approximately 810. As this value is well below the critical threshold for the transition to turbulent flow ($Re < 2300$), the Laminar Flow interface was selected. The continuity equation for an incompressible fluid,

$$\nabla \cdot \mathbf{v} = 0 \quad (3)$$

was solved alongside the Navier–Stokes momentum equation,

$$\rho(\mathbf{v} \cdot \nabla \mathbf{v}) = -\nabla \mathbf{p} + \mu \nabla^2 \mathbf{v} + \mathbf{F}_{Lorentz} \quad (4)$$

where \mathbf{v} is fluid velocity, ρ is density, μ is dynamic viscosity, and $\mathbf{F}_{Lorentz}$ is the electromagnetic body force. To determine the developed pressure of the pump, the boundary conditions

were set with the inlet pressure at 0 Pa (as a reference) and a fixed volumetric flow rate of 3 ml/s at the outlet. This configuration allows the solver to calculate the resulting outlet pressure, which directly corresponds to the pump's developed head ($\Delta P = P_{outlet} - P_{inlet}$). This approach correctly models the progressive pressure buildup from the Lorentz force, which is balanced by hydraulic frictional losses, as visualized in Fig. 10. No-slip boundary conditions were applied to all solid-fluid interfaces.

3.3. Magnetohydrodynamic coupling

The Multiphysics module was employed to couple the “Magnetic and Electric Fields” and “Laminar Flow” interfaces within the MHD framework. In this coupling, the Lorentz force

$$\mathbf{F}_{Lorentz} = \mathbf{J} \times \mathbf{B} \quad (5)$$

acts as a volumetric force in the Navier–Stokes equations, while the fluid motion induces an additional electromotive force term, which modifies the current density as

$$\mathbf{J} = \sigma(\mathbf{E} + \mathbf{v} \times \mathbf{B}) \quad (6)$$

A fully coupled solver sequence iteratively updates the EM and fluid fields until both converge under the MHD conditions. By combining Magnetic and Electric Fields and Laminar Flow interfaces within the Multiphysics environment, this method solves for current density, magnetic flux density, and fluid velocity in a single MHD framework.

3.4. Thermal analysis

A steady-state thermal analysis was conducted to evaluate the temperature distribution of the pump body resulting from Ohmic heating. The analysis solved the heat conduction equation, using the volumetric heat source term imported directly from the converged MHD simulation. The convective cooling effect from the internal fluid flow was coupled by importing the velocity field from the MHD results. A constant temperature of 200 °C was applied at the fluid inlet. To ensure a conservative estimation, natural convection and radiation from the pump's external surfaces were neglected.

3.5. Mesh

Fig. 5 shows the mesh design employed in this study, consisting of 974,393 elements. A mesh independence test was performed to ensure that the simulation results remain stable beyond a certain mesh density. Table 1 presents the mesh independence study, from which the M3 mesh setting was selected as an optimal compromise between accuracy (3.3 %

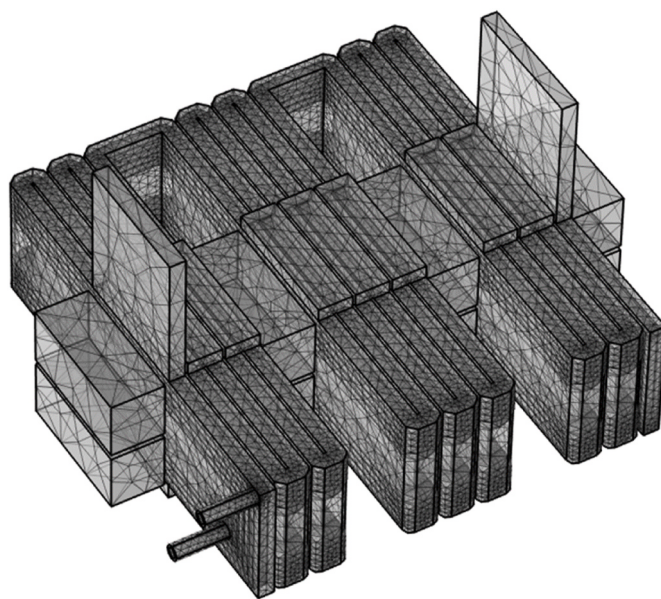


Fig. 5. Mesh configuration used in this study (974,393 elements, M3).

Table 1
Mesh independence study based on the number of elements.

Elements number	Developed pressure [bar]	Percentage error
M1: 2,156,090	10.18	–
M2: 1,454,723	10.20	0.2
M3: 974,393	10.52	3.3
M4: 705,206	11.04	8.4
M5: 547,002	11.95	17.4

error) and computational time.

3.6. Comparison with existing experimental data

To validate the numerical approach used in this study, a simulation was performed using a model that replicates the geometry of the helical-type pump from the reference by Kang [6]. The purpose of this was to verify the accuracy of the simulation framework before applying it to the new design. The referenced study [6] utilized a 4 mm diameter circular

channel, and the maximum Reynolds number under the tested conditions was approximately 1700, confirming the flow was laminar and justifying the use of a laminar flow model. As shown in Fig. 6, the simulation results for the developed pressure show reasonable agreement with the experimental data, with a maximum difference of less than 12 %. This successful validation provides confidence in the reliability of the numerical approach used to predict the performance of the new pump design in the following sections.

4. Results and discussion

To quantitatively investigate the influence of the flow channel geometry and justify the selected design parameters, a parametric study was conducted. The semi-circular channel diameter was varied from 3 mm to 6 mm, while the input current (330 A) and flow rate (3 ml/s) were held constant. Fig. 7 shows the effect of the diameter on the generated Lorentz force pressure, the hydraulic pressure loss, and the developed pressure. The Lorentz force pressure is defined here as the sum of the developed pressure and the hydraulic pressure loss.

The analysis reveals a critical trade-off in the design. The total generated Lorentz force pressure peaks at a diameter of 4 mm. However, as the diameter increases, the hydraulic pressure loss decreases significantly due to the larger flow area. The combination of these two competing effects results in the net developed pressure being maximized at a 5 mm diameter, reaching the target of 10.5 bar. At 6 mm, the performance drops sharply because the wider structure increases the distance between the magnets, weakening the magnetic field and thus reducing the Lorentz force. Therefore, a 5 mm diameter was selected as the optimal dimension for the proposed pump, and all subsequent analyses are based on this geometry.

The electromagnetic aspects of the proposed pump were first analyzed by studying the magnetic flux density and current density distributions. Magnets size of 50 mm × 23 mm × 20 mm (thickness) were arranged to ensure sufficient flux in the flow channel. Each magnet generated flux in either the +y or -y direction, creating a high-flux zone around the channel, as illustrated in Fig. 8. The average magnitude of magnetic flux density on the center of fluid region was 0.2 T, which helped produce the Lorentz force necessary for pumping.

Next, the current density distribution was analyzed at an input current of 330 A. As illustrated in Fig. 9, the majority of the current travels through a designated path near the center of the magnets, whereas some portion escapes along the channel edges, referred to as fringe current. To reduce this unwanted fringe current, the width of the current path was

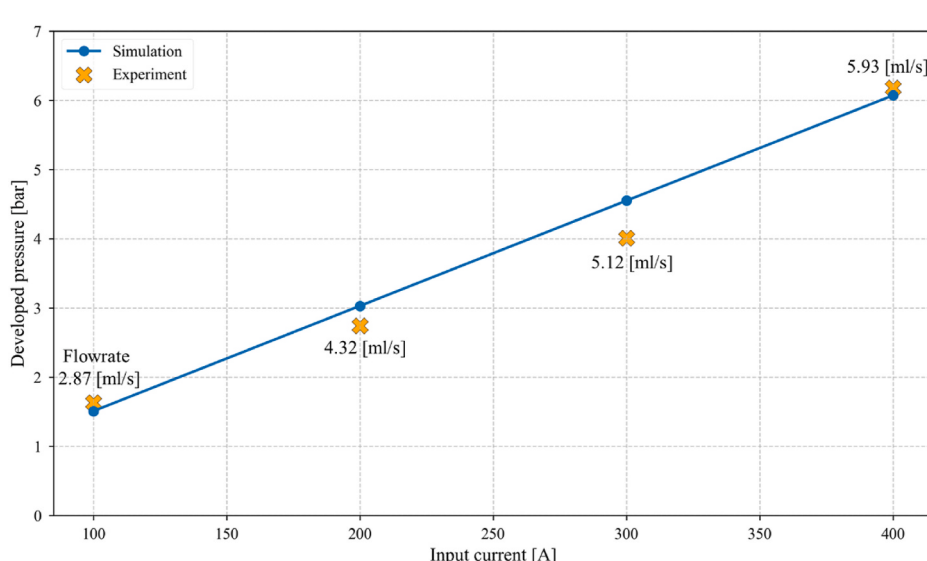


Fig. 6. Simulation validation with helical-type experimental results [6].

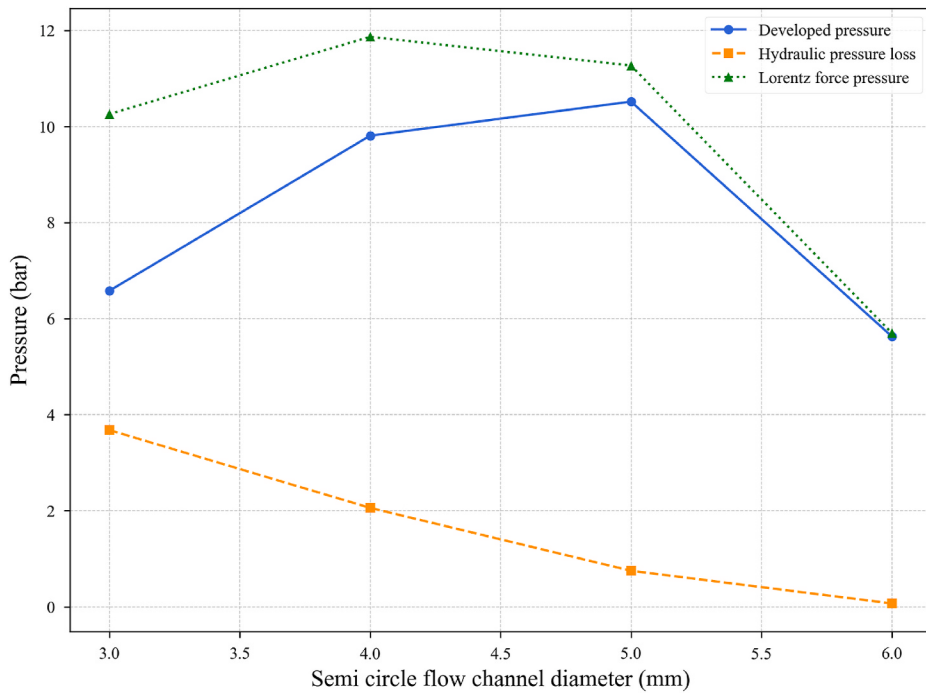


Fig. 7. Effect of flow channel diameter on key pressure components at a 330 A input current and 3 ml/s flow rate.

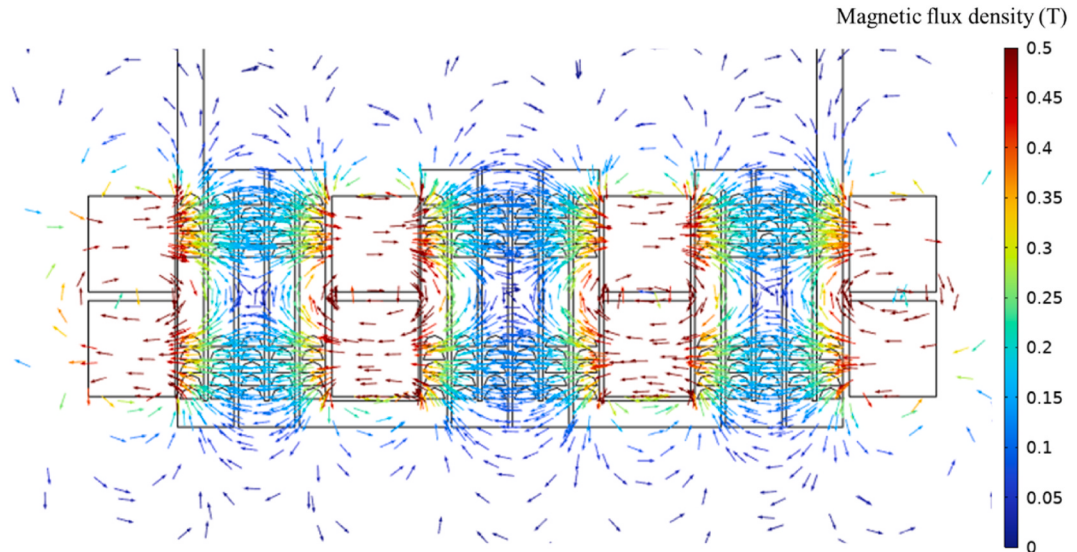


Fig. 8. Magnetic flux density distribution on the yz-plane for the proposed EM pump.

set to 50 mm, matching the magnet width, so that it stays within regions of higher flux density. This arrangement concentrates 67 % of the total current within the central path region, thereby maximizing the effective Lorentz force acting on the fluid and enhancing the pump's capability to generate pressure.

Flow characteristics were evaluated under a fixed inlet flow rate of 3 ml/s, resulting in average velocity of 0.3 m/s. As shown in Fig. 10, at an input current of 330 A the pressure rises progressively along the flow path, reaching 10.5 bar at the pump outlet. This pressure level meets the intended requirement, confirming that the chosen magnet arrangement and current pathway design are effective in producing the desired pumping performance.

In Fig. 11, the pressure–flowrate (P–Q) curve is presented. Consistent with the primary finding of this study, the 330 A curve shows that the

pump develops a pressure of 10.5 bar at a flow rate of 3 ml/s. The consistently negative slope of the P–Q curves indicates stable operation. This is because the pump is self-regulating: a momentary decrease in flow rate causes the pump to generate a higher pressure, creating a surplus that restores the system to equilibrium. Conversely, a momentary increase in flow rate results in a lower pressure, creating a deficit that also pushes the system back toward its stable operating point. This self-correcting mechanism prevents unstable oscillations and ensures reliable performance.

The thermal performance of the pump was analyzed to ensure the permanent magnets operate within a safe temperature range, as excessive heat can degrade their performance. Fig. 12 shows the steady-state temperature distribution of the pump body, resulting from Ohmic losses at a 330 A input current. The analysis was performed under conservative

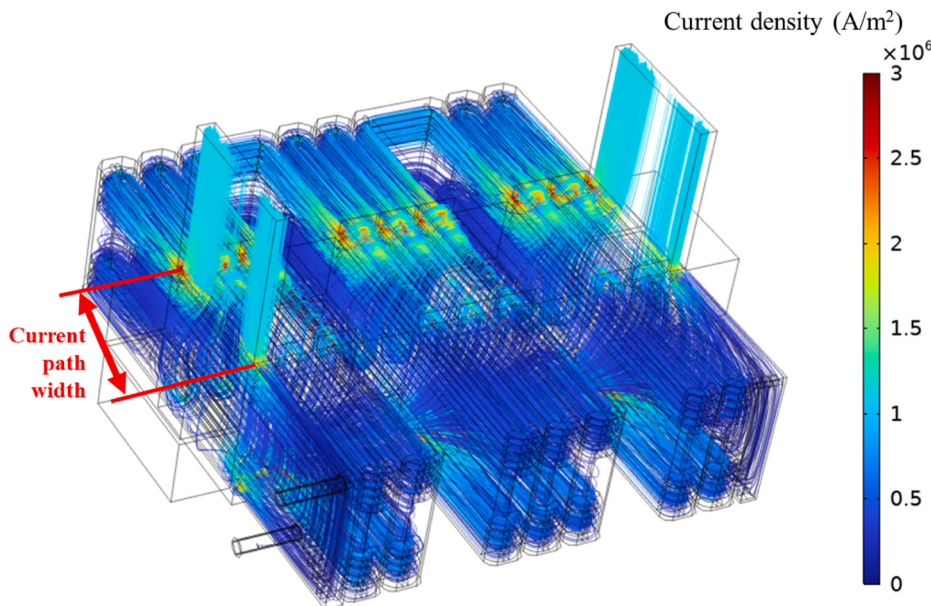


Fig. 9. Current density streamlines in the proposed EM pump at 330 A input current.

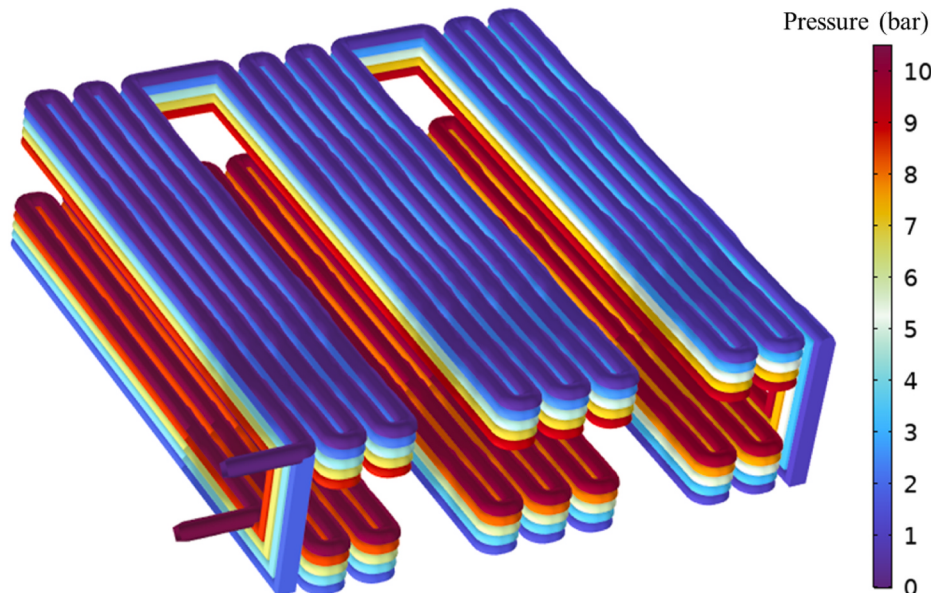


Fig. 10. Pressure distribution of the proposed EM pump at 330 A input current.

assumptions, as detailed in the Methods section.

The maximum temperature of 369 °C is localized at the electrodes, which are uncooled in this model. The key temperature to consider, however, is in the regions adjacent to the permanent magnets. The simulation shows that these surfaces reach a maximum temperature of 288 °C. The selected Sm₂Co₁₇ permanent magnets have a maximum operating temperature of 350 °C. Since the calculated temperature near the magnets is well below this limit, the thermal design is confirmed to be robust, ensuring stable magnet performance.

Finally, the performance of the proposed 3D-printable electromagnetic pump was compared with that of a conventional helical-type electromagnetic pump, as shown in Fig. 13. To achieve a developed pressure of 10.5 bar at a flow rate of 3 ml/s, the 3D-printable pump required 330 A at an input voltage of 0.48 V, whereas the helical-type pump needed 684 A at 0.22 V under the same fluid flow conditions. This represents a 52 % reduction in current demand with similar power

consumption. Additionally, the 3D-printable design reduces the pump's size from 123 mm × 195 mm × 405 mm (helical-type) to 166 mm × 195 mm × 106 mm (3D-printable). These improvements are achieved through multiple optimized current paths and refined flow-channel geometry, enhancing the net Lorentz force applied to the fluid. Furthermore, the additive manufacturing approach simplifies the fabrication process by eliminating complex assembly steps such as brazing, thus improving manufacturability and reliability. Consequently, the compact form factor and simplified fabrication process of the proposed pump increase its potential applicability in constrained spaces typical of SMR coolant loops and accelerator beam-line environments.

To further benchmark the performance against other novel designs, the proposed pump was compared with the high-performance layered stack DC electromagnetic pump developed by Zhang et al. [23]. Their pump achieved a maximum pressure head of 1.2 bar at 300 A. In comparison, the pump in this study generates a substantially higher pressure

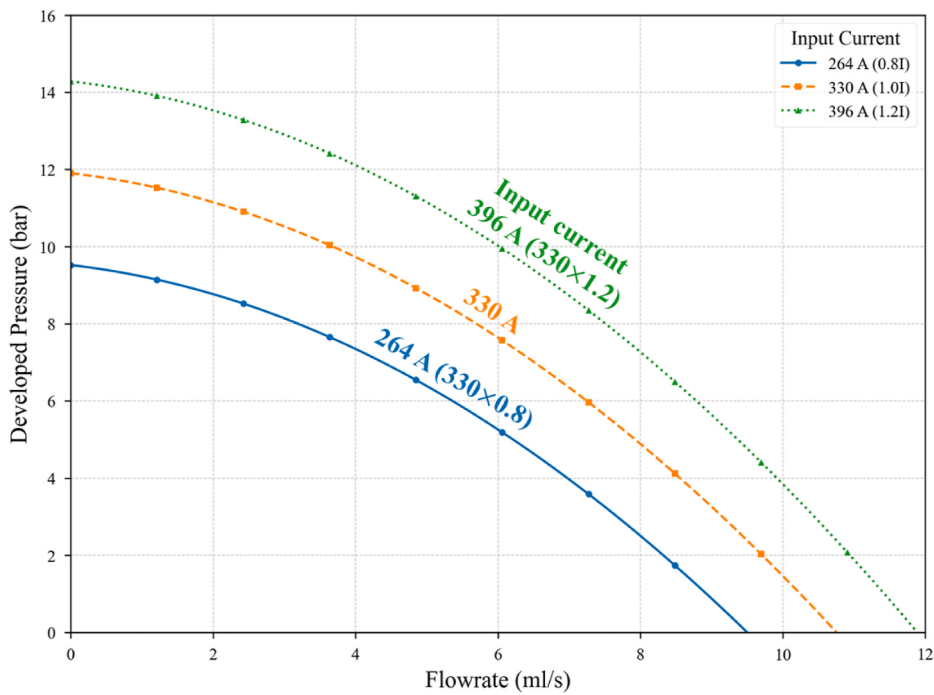


Fig. 11. P-Q curve of the proposed EM pump.

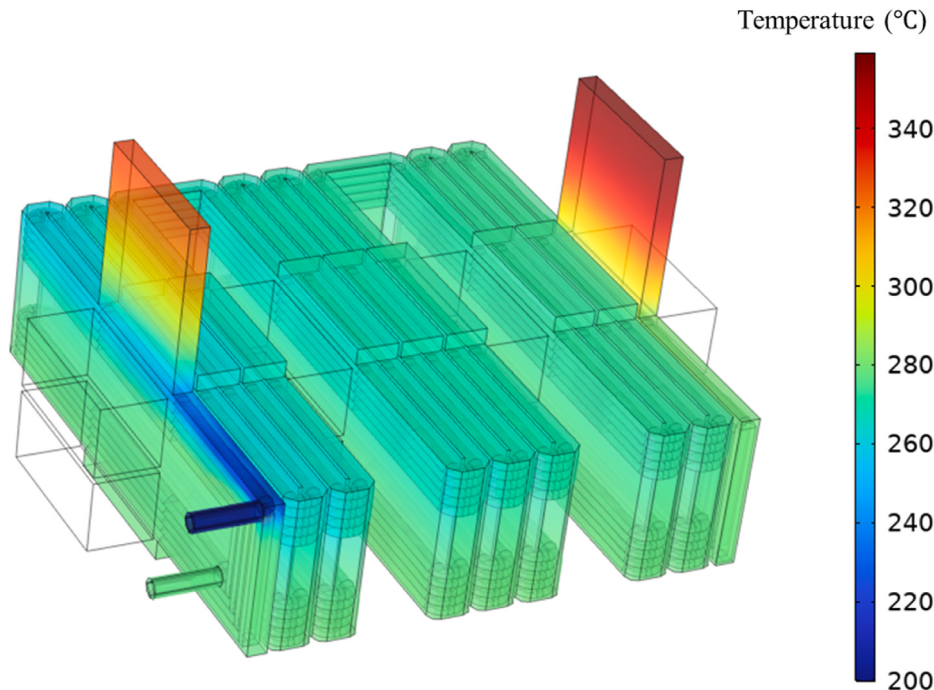


Fig. 12. Temperature distribution of the 3D-printable EM pump at 330 A input current.

of 10.5 bar at an input current of 330 A. This comparison focuses on the low-flow-rate operating point where performance is dominated by the generated Lorentz force, with minimal influence from fluid dynamic losses. As the electrical conductivities of the two working fluids are comparable (3.4×10^6 S/m vs 3.93×10^6 S/m), this significant enhancement in pressure is primarily attributed to the novel pump topology.

5. Conclusion

This study proposed a novel conceptual design for a 3D-printable DC electromagnetic pump to overcome the high current demands and fabrication complexities typically associated with conventional helical-type electromagnetic pumps. By systematically optimizing the arrangement of permanent magnets and current-path geometry, the proposed pump achieved a developed pressure of 10.5 bar at a significantly reduced current input of 330 A, approximately 52 % lower than the 684 A required by a comparable helical-type pump under identical

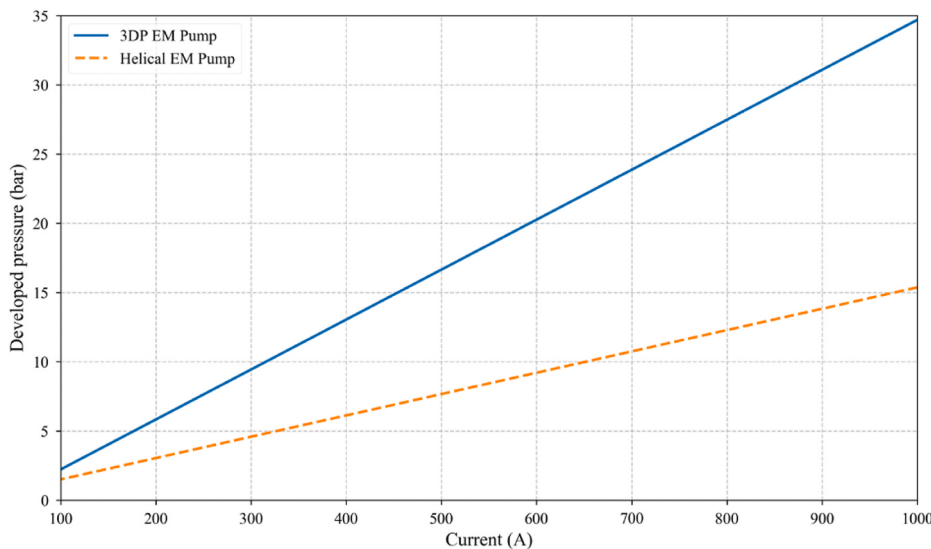


Fig. 13. Pressure comparison between the 3D-printable and helical-type EM pumps according to the input current at a 3 ml/s flowrate.

operating conditions. The use of metal additive manufacturing eliminates the need for brazed joints, simplifying fabrication, reducing potential mechanical failure points, and enabling a more compact pump design. These advantages enhance both cost-effectiveness and ease of manufacturing, making the design potentially suitable for demanding applications such as coolant circulation in sodium-cooled SMRs and liquid-metal charge stripper systems in accelerator. Future research will include experimental validation to investigate the influence of surface roughness in 3D-printed components on MHD performance. Additionally, artificial intelligence techniques will be applied to optimize flow-channel geometry, aiming to further enhance the pump's efficiency and overall performance.

Data availability statement

The datasets generated during and/or analyzed during the current study are available from the corresponding author on reasonable request.

Declaration of competing interest

The authors declare that they have no known competing financial interests or personal relationships that could have appeared to influence the work reported in this paper.

References

- [1] M. Shutayfi, A. Raj, J. Eapen, S. Shannon, Design, modeling, and analysis of a compact-external electromagnetic pumping system for pool-type liquid metal-cooled fast reactors, *Ann. Nucl. Energy* 193 (2023) 109997.
- [2] R. Altamimi, M.S. El-Genk, Miniature DC electromagnetic pumps of molten lead and sodium to support development of Gen-IV nuclear reactors, *Nucl. Eng. Des.* 410 (2023) 112376.
- [3] J. Kwak, H.R. Kim, Modelling and analysis of extra vessel electromagnetic pump for a small modular lead-bismuth fast reactor, *Ann. Nucl. Energy* 152 (2021) 107979.
- [4] C. Liu, Z. He, High heat flux thermal management through liquid metal driven with electromagnetic induction pump, *Front. Energy* 16 (2022) 460–470.
- [5] T.U. Kang, J.S. Kwak, H.R. Kim, Optimization of an extra vessel electromagnetic pump for lead-bismuth eutectic coolant circulation in a non-refueling full-life small reactor, *Nucl. Eng. Technol.* 54 (2022) 3919–3927.
- [6] T.U. Kang, G. Lee, H.R. Kim, Experimental characterization of the flowline of a lithium film formed using an electromagnetic thruster for a RAON prototype charge stripper, *Nucl. Eng. Des.* 412 (2023) 112481.
- [7] S.M. Cho, B.G. Thomas, Electromagnetic forces in continuous casting of steel slabs, *Metals* 9 (2019) 471.
- [8] V. Flikken, Increasing the efficiency of refining and modification of aluminum alloys when using electromagnetic factors, *Magnetohydrodynamics* 58 (2022) 151–156.
- [9] J. Ye, P. Qin, Z.R. Xing, Y. Fan, J.Y. Gao, Z.S. Deng, J. Liu, Liquid metal hydraulic actuation and thermal management based on rotating permanent magnets driven centrifugal pump, *Int. Commun. Heat Mass Tran.* 139 (2022) 106472.
- [10] X.D. Zhang, X.H. Yang, Y.X. Zhou, W. Rao, J.Y. Gao, Y.J. Ding, Q.Q. Shu, J. Liu, Experimental investigation of gallinstan based minichannel cooling for high heat flux and large heat power thermal management, *Energy Convers. Manag.* 185 (2019) 248–258.
- [11] X.D. Zhang, Analytical and Computational Heat Transfer of Single-Phase Liquid Metal, *Handbook of Liquid Metals*, Springer, Singapore, 2024.
- [12] L. Yao, X.B. Li, H.N. Zhang, L.X. Chen, F.C. Li, A novel Halbach array electromagnetic pump for liquid metal flow: design proposal and performance analysis, *Ann. Nucl. Energy* 183 (2023) 109641.
- [13] P. Sun, C.K. Liu, Z.Z. He, A compact double-spiral electromagnetic pump for liquid metal cooling, *Ann. Nucl. Energy* 180 (2023) 109486.
- [14] G. Lee, H.R. Kim, Numerical investigation and comparison of the rectangular, cylindrical, and helical-type DC electromagnetic pumps, *Magnetohydrodynamics* 53 (2) (2017) 429–438.
- [15] M. Dehghan, M. Tahmasebipour, Fabrication of peristaltic electromagnetic micropumps using the SLA 3D printing method from a novel magnetic nanocomposite material, *Sens. Actuators A Phys.* 358 (2023) 114431.
- [16] M. Tahmasebipour, S. Ebrahimi, M. Dehghan, F. Anousheh, A dual-parallel chamber electromagnetic micropump fabricated using 3D printing method from a novel magnetic nanocomposite material, *Int. J. Precis. Eng. Manuf.* 26 (2025) 209–216.
- [17] M. Sedky, M. Serry, High efficiency 3D printed electromagnetic micropump with a synchronous active valve, *Sens. Actuators A Phys.* 341 (2022) 113570.
- [18] M. Rouby, P. Blanchard, P. Lacombe, B. Baroux, G. Beranger, Physical and Mechanical Properties of Stainless Steels, Les Editions de Physique, Les Ulis Cedex A, France, 1993, p. 139.
- [19] C.S. Kim, Thermophysical Properties of Stainless Steels, ANL-75-55, Argonne National Laboratory, 1975.
- [20] S.J. Zinkle, Summary of physical properties for lithium, Pb-17Li, and (LiF)n-BeF₂ coolants, in: APEX Study Meeting, Sandia National Laboratories, 1998, pp. 1–8.
- [21] C.Y. Ho, R.W. Powell, P.E. Liley, Thermal conductivity of the elements, *J. Phys. Chem. Ref. Data* 1 (1972) 279–421.
- [22] A.B. Comsol, COMSOL Multiphysics User's Guide, COMSOL AB, Stockholm, Sweden, 2014, Version 6.2.
- [23] X.D. Zhang, Y.X. Zhou, J. Liu, A novel layered stack electromagnetic pump towards circulating metal fluid: design, fabrication and test, *Appl. Therm. Eng.* 179 (2020) 115610.